Nucleic Acids Research, 2000, Vol. 28, No. 13 **2481–2493**

Structure-based predictions of Rad1, Rad9, Hus1 and Rad17 participation in sliding clamp and clamp-loading complexes

Ceslovas Venclovas* and Michael P. Thelen

Molecular and Structural Biology Division, Biology and Biotechnology Research Program, Lawrence Livermore National Laboratory, L-448, PO Box 808, Livermore, CA 94550, USA

Received March 27, 2000; Revised and Accepted May 5, 2000

DDBJ/EMBL/GenBank accession no. AF247970

ABSTRACT

The repair of damaged DNA is coupled to the completion of DNA replication by several cell cycle checkpoint proteins, including, for example, in fission yeast Rad1^{Sp}, Hus1^{Sp}, Rad9^{Sp} and Rad17^{Sp}. We have found that these four proteins are conserved with protein sequences throughout eukaryotic evolution. Using computational techniques, including fold recognition, comparative modeling and generalized sequence profiles, we have made high confidence structure predictions for the each of the Rad1, Hus1 and Rad9 protein families (Rad17^{Sc}, Mec3^{Sc} and Ddc1^{Sc} in budding yeast, respectively). Each of these families was found to share a common protein fold with that of PCNA, the sliding clamp protein that tethers DNA polymerase to its template. We used previously reported genetic and biochemical data for these proteins from yeast and human cells to predict a heterotrimeric PCNA-like ring structure for the functional Rad1/Rad9/Hus1 complex and to determine their exact order within it. In addition, for each individual protein family, contact regions with neighbors within the PCNA-like ring were identified. Based on a molecular model for Rad17^{Sp}, we concluded that members of this family, similar to the subunits of the RFC clamp-loading complex, are capable of coupling ATP binding with conformational changes required to load a sliding clamp onto DNA. This model substantiates previous findings regarding the behavior of Rad17 family proteins upon DNA damage and within the RFC complex of clamp-loading proteins.

INTRODUCTION

DNA damage, strand breaks and replication errors arising during cell division must be corrected to ensure faithful replication of the genome. This crucial process is carried out by a complex network of proteins, many of which are directly linked to the transmission of cell cycle checkpoint signals. The set of Rad checkpoint proteins, including Rad1^{Sp}, Rad3^{Sp}, Rad9^{Sp}, Rad17^{Sp}, Rad26^{Sp} and Hus1^{Sp}, are important in coupling the repair of DNA damage with DNA replication during the cell cycle (1–4). However, the molecular details of how these proteins function remain unclear.

A recent study has demonstrated that Rad24^{Sc} (Rad17 family) associates specifically with four of the five members of the replication factor C (RFC) complex, RFC$_{2–5}$ (5). Rad17^{Sp} and the RFC$_3$ subunit were found in the same protein complex (6), indicating that association of Rad17 family members with RFC$_{2–5}$ is not confined to budding yeast. Normally the RFC$_{1–5}$ complex facilitates genome replication by loading the sliding clamp protein PCNA onto the targeted site of DNA polymerization (7). The appearance of DNA damage in the cell causes translocation of Rad17^{Hs} out of the nucleolus (8), where it likely exchanges into the RFC complex. Sequence similarities of Rad17^{Sp} and Rad24^{Sc} (9,10) with the RFC clamp-loading subunits have been noted that could explain this exchange. Furthermore, a tentative or transient interaction has been observed between Rad17 and Rad1 in both *Schizosaccharomyces pombe* (4) and human (11) cells. Note, however, that this has not always been observed when tested (12), indicating that this interaction is either weak or dependent on the presence of specific DNA structures.

Another distinct checkpoint protein complex consists of the Rad1, Rad9 and Hus1 proteins in humans (12,13) and *S.pombe* (4) and the functional analogs Rad17^{Sc}, Ddc1^{Sc} and Mec3^{Sc} in *Saccharomyces cerevisiae* (14,15). Although a low degree of sequence similarity has been observed between these *S.cerevisiae* proteins and each of the respective protein families, establishing true homology has been elusive and has remained an open question.

In a previous study we found that the Rad1 family, including the founding member Rec1^{Um} of *Ustilago maydis*, Rad1^{Sp}, Rad17^{Sc} and three other homologs previously culled from cDNA and genome databases, are distantly related to the PCNA protein structure (16). This finding stimulated the notion that Rad1 might act as a sliding clamp during DNA

*To whom correspondence should be addressed. Tel: +1 925 422 3097; Fax: +1 925 422 2282; Email: venclovas@llnl.gov
Permanent address:
Ceslovas Venclovas, Institute of Biotechnology, Graiciuno 8, 2028 Vilnius, Lithuania

repair-dependent replication. Importantly, Hus1 was also recently found to be homologous to both Rad1 and PCNA (17). These unexpected observations were followed by the addition of $Rad9^{Sp}$ to the list of putative PCNA homologs (4,18).

Here we report the results of using a range of computational methods to examine more closely the relationship of these three protein families to the available structures of other proteins. In doing so we have verified the sequence and structural similarities of all three families with PCNA, including a close inspection of the divergent *S.cerevisiae* protein members. We have also modeled the putative ATP-binding site of $Rad17^{Sp}$ based on the experimental structures of bacterial clamp-loading protein δ′ and the *N*-ethylmaleimide-sensitive fusion (NSF) protein in the ATP-bound state. From these structure-based predictions, we propose a mechanism by which Rad17/$RFC_{2–5}$ and the Rad1/Rad9/Hus1 proteins interact to facilitate the repair of DNA damage during the crucial DNA synthesis stage of the cell division cycle.

MATERIALS AND METHODS

PSI-BLAST searches

PSI-BLAST (19) searches were performed against the non-redundant sequence database at the NCBI (www.ncbi.nlm.nih.gov). For the Rad1, Rad9 and Hus1 protein families, PSI-BLAST searches were run using default parameters until profile convergence. For the Rad17 family the number of matching protein sequences was very large. Therefore, instead of running searches until profile convergence, we limited iteration to between four and six cycles.

Identification of *Caenorhabditis elegans Rad9*

After finding an initial sequence match to the Rad9 protein family, a *Rad9*-like gene (GenBank accession no. AF247970) from *C.elegans* was predicted using the Gene Finder program suite (URL: http://dot.imgen.bcm.tmc.edu:9331/gene-finder/gfb.html) and monitoring protein sequence homology with other Rad9 proteins. Full-length $Rad9^{Ce}$, encoding a protein of 323 residues, is most similar within this family to $Rad9^{Hs}$ (~21% identity as determined after multiple sequence alignment of Rad9 family members) and although the actual C-terminus is uncertain, the predicted sequence completely encompasses the region assigned as the PCNA-like fold in other Rad9 proteins.

Multiple sequence alignments

Alignment of multiple sequences was performed with the PILEUP program (GCG Inc., Madison, WI) using the Blosum50 substitution matrix (20). In each case, a series of alignment variants were produced by gradually lowering the gap opening and extension penalties from the default values. The final alignment of multiple sequences was constructed by taking the dominant variant for each region. When the alignment of a particular subsequence was highly dependent on gap penalties, this region was aligned manually using PSIPRED (21) secondary structure predictions for individual sequences as a guide.

Sequence–structure threading

Compatibility of individual sequences with known 3-dimensional (3D) protein structures was tested using the sequence–structure threading method developed by Fischer and Eisenberg (22; URL: http://fold.doe-mbi.ucla.edu/). Briefly, the sequence of interest ('probe') is threaded onto every fold in a library of structures. Every resulting sequence–structure pair is then assigned a score, indicating compatibility of the probe sequence with the given fold under the resulting alignment. A noteworthy feature of this particular threading method is that, in addition to the amino acid sequence of the probe, the predicted secondary structure of the probe is used to measure the compatibility with the given fold. To determine significance of the match, or how likely it is that this match arises by chance, the compatibility score is expressed as a *Z* score [the number of standard deviations (σ) above the mean score]. The higher the *Z* score, the more likely it is that the threaded probe adopts the matching fold. A *Z* score $>7\sigma$ indicates a true positive (22). Threading fitness scores were used to evaluate general compatibility of probe sequence with matching structures, while corresponding sequence–structure alignments were used in the molecular modeling procedure given below.

Construction and evaluation of sequence–structure alignments

To further explore the relationship of the Rad9 and Hus1 protein families with PCNA, we have constructed and analyzed the respective sequence–structure alignments. For this purpose we used an iterative model building/evaluation approach similar to that described earlier (23), consisting of three main steps: (i) alignment of a probe sequence with 3D structure(s) of related protein(s); (ii) construction of a corresponding 3D molecular model; (iii) evaluation of the modeled structure. The idea behind this approach is that most of the alignment errors, undetectable at the sequence level, would manifest themselves in the 3D structure and could be identified by model evaluation. Instead of using a single probe sequence as in our earlier study of the Rad1 family (16), several members of both the Rad9 and Hus1 protein families were used as probe sequences to increase the sensitivity of this procedure. Sequence variation within a protein family makes it more likely that an alignment error, which may not be recognized as a significant flaw in the 3D structure in a particular representative, will be identified as such a flaw in other family members.

Rad9 and Hus1 alignments with PCNA. Because of very low sequence similarity of both the Rad9 and Hus1 families to PCNA, construction of the initial Rad9–PCNA and Hus1–PCNA alignments presented considerable challenges. To avoid testing a large number of alignment variants for every structurally conserved region of PCNA, we used an approach designed to provide both a reasonable number of sequence–structure mapping variants as well as an initial assessment of the region-specific confidence of the alignments. In this approach we have used data from two procedures: multiple sequence alignments and pairwise alignments resulting from sequence–structure threading.

The regions of Rad9–PCNA and Hus1–PCNA alignments that displayed the highest stability in both the multiple

Table 1. Orthologous proteins in four cell cycle checkpoint families

Organism	Clamp loader-like	PCNA (clamp)-like		
	Rad17	Rad1	Rad9	Hus1
Human	Rad17^{Hs}	Rad1^{Hs}	Rad9^{Hs}	Hus1^{Hs}
Mouse	Rad17^{Mm}	Rad1^{Mm}	Rad9^{Mm}	Hus1^{Mm}
Fly (*Drosophila melanogaster*)	Rad17^{Dm}	Rad1^{Dm}	Rad9^{Dm}	Hus1^{Dm}
Fission yeast (*S.pombe*)	Rad17^{Sp}	Rad1^{Sp}	Rad9^{Sp}	Hus1^{Sp}
Budding yeast (*S.cerevisiae*)	Rad24^{Sc}	Rad17^{Sc}	Ddc1^{Sc}	***Mec3^{Sc}***
Nematode (*C.elegans*)	Rad17^{Ce}	Rad1^{Ce}	***Rad9^{Ce}***	Hus1^{Ce}
Plant (*Arabidopsis thaliana*)	Rad17^{At}	Rad1^{At}	Rad9^{At}	Hus1^{At}
Fungus (*U.maydis*)	–	Rec1^{Um}	–	–
Plasmodium (*P.polycephalum*)	–	–	–	Lig1^{Pp}
Yeast (*S.octosporus*)	–	–	Rad9St	–
Protozoan (*L.major*)	–	–		Hus1^{Lm}

Indicated in bold italics are Mec3^{Sc}, confirmed in this study as a Hus1 family member with PCNA-like structure, and Rad9^{Ce}, identified here as a hypothetical protein from the *C.elegans* genomic sequence.

Table 2. Threading results for the Hus1 protein family

Sequences threaded	Top three structural matches		
	1	**2**	**3**
Hus1_hs 280a.a.	1PLQ 10.40 DNA clamp	1PLQ 7.17 DNA clamp	1IGS 4.20 β/α (TIM)-barrel
Hus1_mm 281a.a.	1PLQ 9.86 DNA clamp	1AXC 8.53 DNA clamp	1IGS 4.22 β/α (TIM)-barrel
Hus1_dm 278a.a.	1PLQ 4.33 DNA clamp	1AXC 3.93 DNA clamp	1PDA 3.53 Periplasmic binding protein-like II
Hus1_sp 287a.a.	1AXC 13.32 DNA clamp	1PLQ 10.33 DNA clamp	1IGS 4.59 β/α (TIM)-barrel
Hus1_ce 277a.a.	1PLQ 5.54 DNA clamp	1AOD 4.78 β/α (TIM)-barrel	1AXC 4.59 DNA clamp
Lig1_pp 220a.a.	1PLQ 5.90 DNA clamp	1AXC 5.32 DNA clamp	1ZAK 4.78 P-loop containing nucleotide triphosphate hydrolases
Hus1_at 344a.a.	2THI 3.87 Periplasmic binding protein-like II	1BIF 3.60 P-loop containing nucleotide triphosphate hydrolases	1IGS 3.47 β/α (TIM)-barrel

Each structural match is represented by PDB code, fold definition from the SCOP database and the resulting *Z* score. If a sequence matched a structure having domains of different folds, the one with the most extensive match is included. Bold indicates matches with *Z* scores >7.0σ.

sequence alignment study and in the threading-based alignments were compared. Where alignment of these regions in both cases agreed, they were considered reliably aligned and tested as single variants in model building. For the rest of the regions, up to five different alignment variants originating either from multiple sequence alignments, threading or manual alignment were considered.

Construction of molecular models. Every alignment variant for each probe sequence was used to generate a corresponding molecular model. Protein models were constructed with MODELLER (24) using superimposed yeast and human PCNA structures (PDB codes 1PLQ and 1AXC, respectively) as templates. After coordinates were assigned to the probe sequence, side chains were rebuilt with the program SCWRL (25). The quality of the models was then assessed by visual inspection and with ProsaII (26), a method designed to detect errors in 3D structures of proteins. As an indicator of the overall quality of a particular model we have used the ProsaII *Z* score, which is the difference between the empirical energy of the model and the mean energy of many other folds onto which the same sequence is threaded, expressed in units of standard deviation (σ). Particular alignment variants were selected based on the consensus of ProsaII *Z* scores for all

Table 3. Threading results for the Rad9 protein family

Sequences threaded	Top three structural matches					
	1		2		3	
Full length						
Rad9_hs 1-391a.a.	1ARP Heme-dependent peroxidases	5.60	1PLQ DNA clamp	5.56	1ANT Serpins	5.02
Rad9_mm 1-398a.a.	1ARP Heme-dependent peroxidases	5.85	1AXC DNA clamp	5.52	1PLQ DNA clamp	4.88
Rad9_dm 1-456a.a.	1AXC DNA clamp	6.82	1ECF N-terminal nucleophile aminohydrolases (Ntn hydrolases)	5.50	1BO1 SAICAR synthase-like	3.61
Rad9_sp, 1-426a.a.	1AXC DNA clamp	6.32	1FNF Immunoglobulin-like β-sandwich	4.05	1PLQ DNA clamp	4.00
Rad9_st 1-423a.a.	1PLQ DNA clamp	7.48	1AXC DNA clamp	4.66	1GLA Ribonuclease H-like motif	3.65
Ddc1_sc 1-612a.a.	1GOF 7-bladed β-propeller	4.10	1CRL α/β-Hydrolases	3.86	1BTC β/α (TIM)-barrel	3.75
N-terminal deletion						
Rad9_hs 70-391a.a.	1ARP Heme-dependent peroxidases	6.76	1CPO EF Hand-like	4.61	1MNP Heme-dependent peroxidases	4.08
Rad9_mm 70-398a.a.	1ARP Heme-dependent peroxidases	6.70	1TCR Immunoglobulin-like β-sandwich	4.61	1MNP Heme-dependent peroxidases	4.22
Rad9_dm 70-456a.a.	1BO1 SAICAR synthase-like	4.58	1GPH Phosphoribosyltransferases (PRTases)	4.01	1ALK Phosphatase/sulphatase	3.45
Rad9_sp 70-426a.a.	1FNF Immunoglobulin-like β-sandwich	5.00	1ZAP Acid proteases	4.20	2MNR β/α (TIM)-barrel	3.93
Rad9_st 70-423a.a.	1PLQ DNA clamp	5.42	1GLA Ribonuclease H-like motif	4.26	1CPO EF Hand-like	3.72
Ddc1_sc 70-612a.a.	1CRL α/β-Hydrolases	4.36	1BR7 Ubiquitin conjugating enzyme	4.02	2GBP Periplasmic binding protein-like I	3.81
C-terminal deletion						
Rad9_hs 1-280a.a.	1PLQ DNA clamp	8.39	1AXC DNA clamp	5.86	4BLM β-Lactamase/D-ala carboxypeptidase	3.64
Rad9_mm 1-280a.a.	1AXC DNA clamp	7.47	1PLQ DNA clamp	6.81	1LYA/ Acid proteases	4.42
Rad9_dm 1-280a.a.	1AXC DNA clamp	10.03	1CP3 Caspase	5.15	1PLQ DNA clamp	4.76
Rad9_sp 1-306a.a.	1AXC DNA clamp	8.89	1PLQ DNA clamp	6.18	1AOD β/α (TIM)-barrel	5.30
Rad9_st 1-306a.a.	1PLQ DNA clamp	9.12	1AXC DNA clamp	6.32	1AOD β/α (TIM)-barrel	4.41
Ddc1_sc 1-409a.a.	1EMA Green fluorescent protein, GFP	4.70	1NFP β/α (TIM)-barrel	3.85	1AOZ Cupredoxins	3.29

Notation as in Table 2. The results are provided for the complete Rad9 sequences, as well as for truncated forms: N-terminal deletion of 70 residues and lacking poorly conserved C-terminal regions.

probe sequences from the same family (either Rad9 or Hus1). However, in some cases even evaluation of corresponding models was not sufficient to make an unambiguous selection from different alignment variants. These were selected arbitrarily and the corresponding alignment regions were considered to be of lower confidence (indicated by a gray background of secondary structure elements in Fig. 1B and C).

Mec3^{Sc} and Ddc1^{Sc} alignments. Alignments for yeast Mec3^{Sc} and Ddc1^{Sc} proteins were constructed differently from the other sequences of corresponding families. Multiple sequence alignments for the Ddc1^{Sc}–Rad9 family, and even more so for the Mec3^{Sc}–Hus1 family, contained a number of regions which did not produce single dominant alignment variants. For these regions the alignment was constructed either by taking one of the produced alignment variants by aligning manually, guided by PSIPRED (21) secondary structure predictions. Accordingly, these regions were assigned lower alignment confidence. The resulting Mec3^{Sc}–Hus1 and Ddc1^{Sc}–Rad9 family alignments were then simply merged with Hus1–PCNA and Rad9–PCNA structure-based alignments to produce the final multiple sequence alignments shown in Figure 1B and C, respectively.

Profile searches

Sequence profiles were constructed from the multiple sequence alignments using the Pftools package (27; URL: ftp://ftp.isrec.isb-sib.ch/sib-isrec/pftools/). These profiles were used to search against the yeast protein sequence database

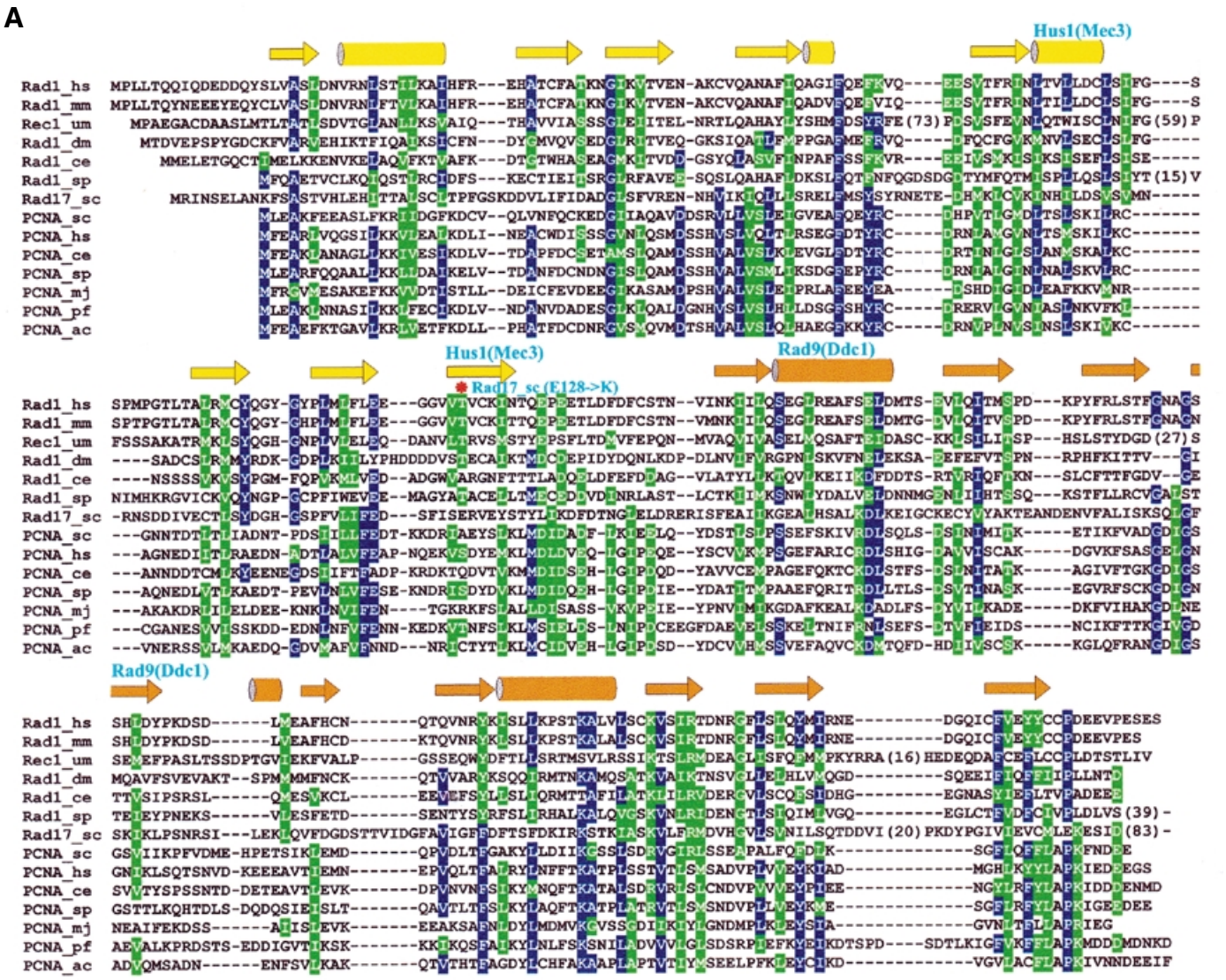

containing the complete yeast genome (www.ncbi.nlm.nih.gov) and subsequently extended by adding all known members of the Rad1, Rad9 and Hus1 families as well as a number of PCNA sequences, representing a broad spectrum of conservation, for reference points.

Modeling the nucleotide-binding site for a Rad17 protein family representative

The Rad17 protein family and the yeast RFC subunits were aligned separately and then merged together as described above. Structures of the δ′ subunit (PDB code 1A5T) of *Escherichia coli* DNA polymerase III and NSF D2 (1D2N) were superimposed. Structurally equivalent regions in the δ′ subunit corresponding to ATP-binding motifs in NSF D2 were identified and four motifs that could be aligned unambiguously with both the Rad17 family and RFC proteins were selected. The structure of NSF D2 was then used as a template to model the structural arrangement of these four sequence motifs in Rad17^{Sp}. The model of the Rad17^{Sp} nucleotide-binding site was constructed by substituting non-conserved side chains while preserving the NSF D2 backbone conformation as well as the spatial position of the bound ATP analog and magnesium ion.

RESULTS AND DISCUSSION

A thorough search of the sequence databases yielded several new members of the Rad1, Rad9, Hus1 and Rad17 cell cycle checkpoint protein families, indicating the wide extent of conservation in these checkpoint mechanisms. The evolutionary and structural relationships of proteins within each of the families examined in our study are given in Table 1. The table partly summarizes the results of this study and also addresses the issue of considerably confusing nomenclature for these four protein families.

Identification of the PCNA fold in the Rad1, Rad9 and Hus1 families

All members of the Rad1 protein family were predicted by comparative modeling to have the PCNA fold (16). As judged

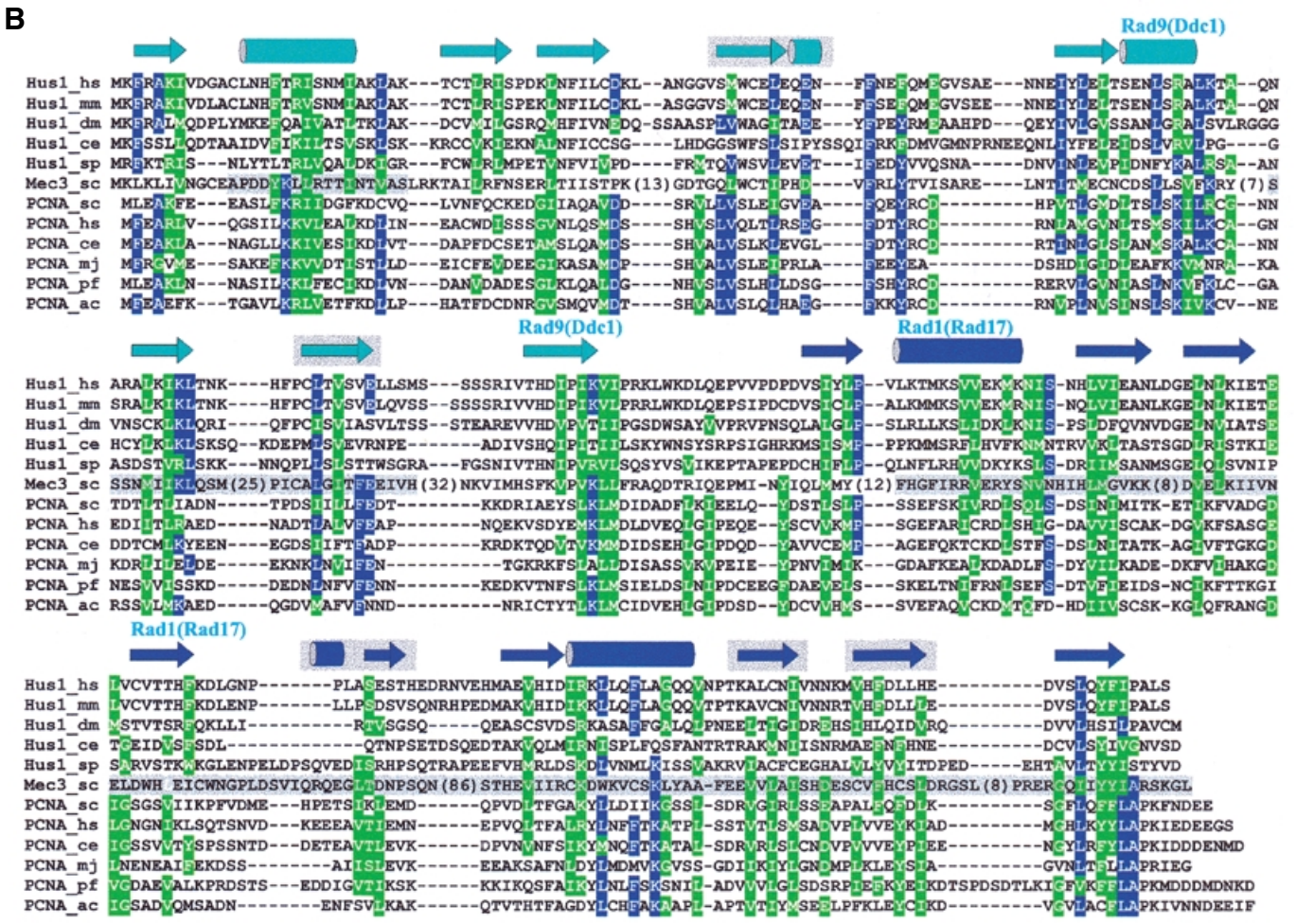

by the results of an iterative PSI-BLAST search, at least three Hus1 homologs appear to be related to both Rad1 and to PCNA (17). However, when each Hus1 family member (Table 1) was run independently as a probe in a PSI-BLAST search, PCNA was never picked up above the *E*-value threshold. We therefore used sequence–structure threading (22) to test the relationship between Hus1 and PCNA. Each Hus1 protein sequence was tested for compatibility with all known 3D structures and found to consistently match PCNA better than any other protein structure (Table 2). The resulting sequence–structure alignments spanned the entire length of PCNA, giving additional support for the structural similarity between the Hus1 and PCNA families.

As with Hus1, PSI-BLAST searches performed for each of the Rad9 family proteins did not detect significant sequence similarity with proteins other than members of the Rad9 family. Again, individual Rad9 sequences were threaded against a library of 3D protein structures and PCNA was identified as a strong candidate fold (Table 3). Nevertheless, threading results for Rad9 proteins were not as consistent as for Hus1 proteins. As this appeared to result from additional length in all Rad9 protein sequences, we decided to test the idea that poorly conserved C-terminal regions extend beyond the PCNA fold encompassed by much stronger conserved N-terminal regions. In agreement with this idea, truncation of C-termini made PCNA the dominant matching fold with very high fitness scores. In contrast, PCNA almost completely disappeared from the list of best matches if the threaded Rad9 sequences lacked the N-terminal 70 residues.

Since only PCNA structures matched with *Z* scores greater than the threshold (7σ) established independently for false positives (22), threading results leave little doubt that proteins from the Rad1, Rad9 and Hus1 families all possess the PCNA fold. At the same time, it is known that detection of distant homologs either by sequence searches or by threading does not necessarily translate into correct, structurally sound sequence alignments (28,29). This seemingly contradictory observation is consistent with the idea that a protein fold is primarily determined by global sequence characteristics and is not localized to particular residues (30). We considered alignment accuracy and estimation of its reliability especially important since these alignments will be used as a guide for experimental studies at the residue level, such as site-specific mutagenesis. To avoid errors in the alignment of PCNA with these particular Rad checkpoint protein sequences, molecular models were constructed with full atom representation for proteins from both the Hus1 and Rad9 families. Modeling was used to address the independent verification of threading, refinement

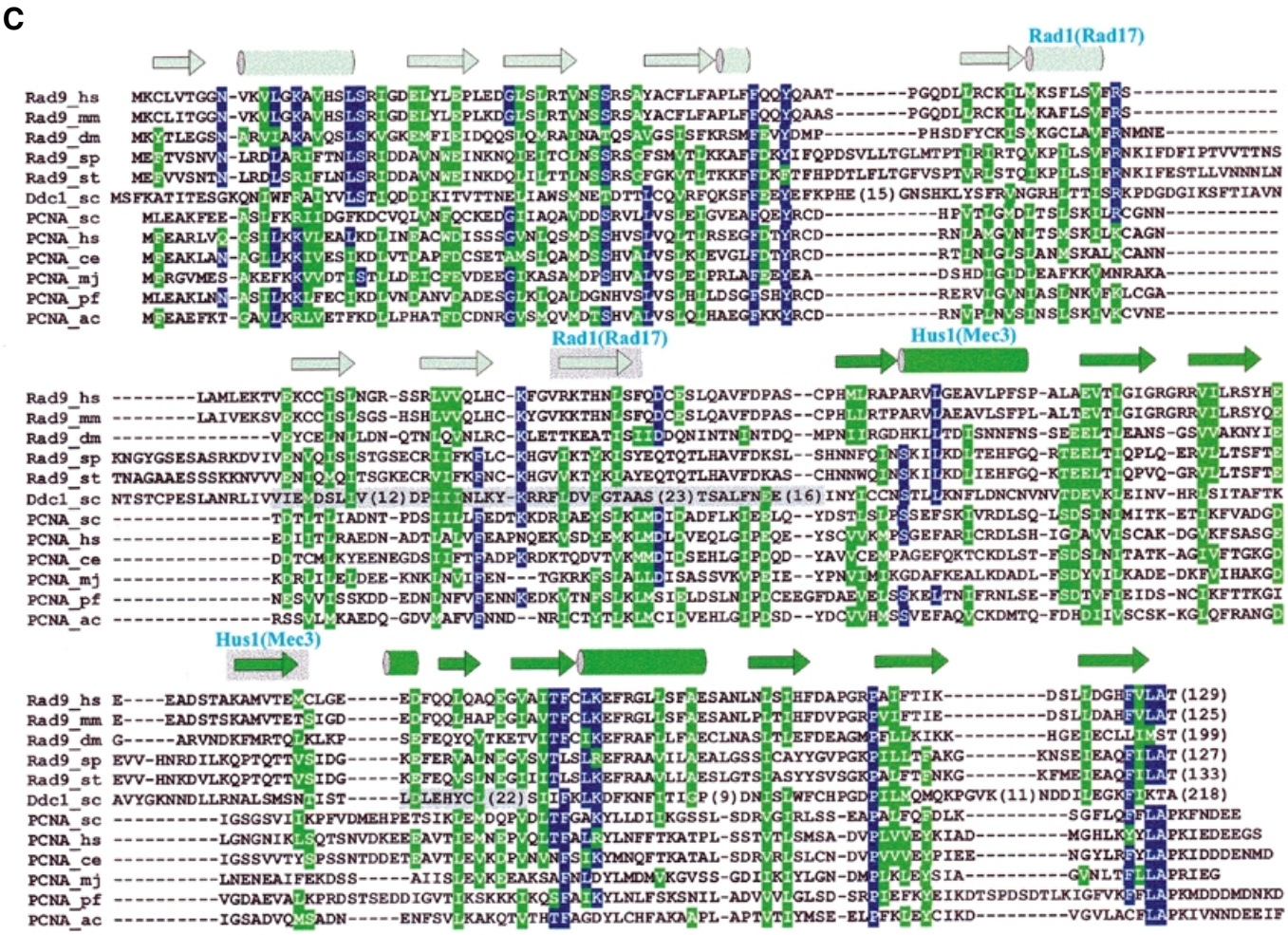

Figure 1. (Previous two pages and above) Sequence–structure alignments of Rad checkpoint proteins with PCNA: (**A**) Rad1–PCNA, (**B**) Hus1–PCNA and (**C**) Rad9–PCNA. Residues conserved in sequences of more than a single family are colored blue (identical) and green (similar). Secondary structure of yeast PCNA is shown by arrows (strands) and cylinders (helices) for each alignment with different coloring representing two structural domains in a PCNA monomer. Regions of Rad1, Hus1 and Rad9 proteins involved in forming interfaces between monomers in the heterotrimeric ring structure (Fig. 2) are denoted by names of the interacting partners above the secondary structure elements. In the Rad1–PCNA alignment (A) the E128K mutation preventing formation of the $Rad17^{Sc}$–$Mec3^{Sc}$ complex is also indicated (*). A shaded background for some secondary structure elements indicates that the sequence–structure alignment in corresponding regions is less confident. Shading in $Mec3^{Sc}$ (B) and $Ddc1^{Sc}$ (C) sequences mark regions of uncertainty in their alignment with, respectively, the Hus1 and Rad9 families. Long insertions and C-terminal regions extending beyond the PCNA fold were removed to preserve space and numbers in parentheses indicate the lengths of removed fragments.

of sequence–structure alignments with PCNA and estimation of region-specific reliability of the alignments. The resulting sequence–structure alignments between representatives of the Rad1, Rad9 and Hus1 families with PCNA proteins are displayed with the indicated region-specific confidence (Fig. 1).

The general fitness of any particular sequence aligned to the PCNA scaffold is indicated by the results of model evaluation with ProsaII (Table 4). Native-like protein structures are assigned lower energy (and corresponding lower *Z* scores). Because the ProsaII *Z* score depends on the length of the protein chain, we have included *Z* scores for experimentally determined and modeled structures of similar size to have reference points for both correct and flawed protein structures. Experimental structures include both yeast and human PCNA, which were used as structural templates to obtain models. Two other reference structures are models of the first two domains of the β subunit of *E.coli* polymerase III, a known structural and functional homolog of PCNA. Both models were generated using yeast PCNA as the structural template, but one model (β) was based on accurate structure-based alignment, while the second (β*) was based on a previously reported incorrect alignment (31). All models of Rad1 (16), Rad9 and Hus1 proteins were assigned *Z* scores better than that for the correctly aligned β model and close to those assigned to native PCNA structures. These results indicate with high certainty that Rad1, Rad9 and Hus1 proteins fold into PCNA-like structures and that the sequence–structure alignments in most regions are likely to be correct.

Table 4. ProsaII evaluation of protein structures

Protein structure	ProsaII *Z* score (σ)
Rad9 and Hus1 models	
Rad9_hs	–7.33
Rad9_mm	–8.13
Rad9_dm	–7.42
Rad9_sp	–7.02
Rad9_st	–7.78
Hus1_hs	–8.04
Hus1_mm	–8.22
Hus1_dm	–8.31
Hus1_ce	–7.36
Hus1_sp	–7.51
Reference structures	
Yeast PCNA (1plq)	–10.42
Human PCNA (1axc)	–9.26
β model (correct alignment)	–6.81
β* model (wrong alignment)	–0.36

Homology of the Rad17^{Sc}, Ddc1^{Sc} and Mec3^{Sc} proteins

Establishing homology of checkpoint proteins from *S.cerevisiae* to proteins from other species has been especially challenging. The protein complex containing Rad1, Rad9 and Hus1 in human cells (12,13) and *S.pombe* (4) is functionally analogous to that observed in *S.cerevisiae*, containing Rad17^{Sc}, Ddc1^{Sc} and Mec3^{Sc} (14,15). Rad17^{Sc} is an ortholog of the Rad1 family (32,33) and Ddc1^{Sc} was suggested to be distantly related to Rad9^{Sp} (34). Recently, Mec3^{Sc} was tentatively assigned to the Hus1 family, but no PCNA-like motifs were detected (4). To test for the evolutionary relationship of Mec3^{Sc}, we used generalized sequence profiles (27) of aligned Hus1 sequences to search the entire translated *S.cerevisiae* genome. Profiles constructed from Hus1 family members alone and from the sequence–structure Hus1–PCNA alignment (Fig. 1B) turned up Mec3^{Sc} as the most similar yeast protein sequence (discounting yeast PCNA in the latter case, as it was used in profile construction). Mec3^{Sc} matched the latter profile even better than PCNA sequences from some other organisms. These results clearly indicate that Mec3^{Sc} is related to the Hus1 family and that it has recognizable sequence similarity to PCNA. Interestingly, searching with the Hus1–PCNA profile turned up proteins from both the Rad1 and Rad9 families, although these had somewhat lower scores. Profiles constructed from the Rad1–PCNA (Fig. 1A) and Rad9–PCNA (Fig. 1C) alignments retrieved proteins from the Rad9/Hus1 and Rad1/Rad9 families, respectively (including those from *S.cerevisiae*), with sufficiently high scores. This provided supplementary evidence for the predicted evolutionary relationship between the Rad1, Rad9, Hus1 and PCNA protein families.

Because Ddc1^{Sc} and especially Mec3^{Sc} are very divergent from the corresponding proteins in the Rad9 and Hus1 families, these alignments are less reliable. Nevertheless, after producing Ddc1^{Sc} and Mec3^{Sc} alignments (see Materials and Methods) it became obvious that the relationship of these two proteins with the Rad9 and Hus1 families is camouflaged by a number of long insertions. Whereas similarity to PCNA was not recognized with full-length Ddc1^{Sc} and Mec3^{Sc} sequences, removing these lengthy insertions prior to threading resulted in bringing PCNA to the number one matching position.

The structure predictions for the Rad1, Rad9 and Hus1 families utilized several complementary methods. The threading approach used here to a large degree relies on how well predicted secondary structure for the probe sequence fits the structural template. At the same time, ProsaII evaluation takes into account residue–residue interactions, comparing them to the ones observed in experimentally determined structures. Sequence profiles use only conservation patterns of aligned sequences. The fact that all three methods strongly support evolutionary relationships between the Rad1, Rad9, Hus1 and PCNA families greatly increases the reliability of this finding.

Heterotrimeric ring structure of the Rad1/Rad9/Hus1 complex

Our earlier finding that the Rad1 family is related to PCNA led to the hypothesis that Rad1 forms a PCNA-like clamp involved in damage-specific processing of DNA (16). However, more recent evidence indicates that overexpressed, purified Rec1^{Um} (35) and Rad1^{Hs} (M.P.Thelen, unpublished results) proteins exist in solution as monomers, not as homotrimers as we postulated. On the other hand, genetic studies showed that cells fail to activate the DNA damage checkpoint if at least one of Rad1, Rad9 or Hus1 is non-functional (3). Furthermore, recently, all three proteins were found within a distinct protein complex in both humans and yeasts (4,12–15) and formation of such a complex is critical for activating the DNA damage checkpoint (14). Since members of the Rad1, Rad9 and Hus1 families all appear to possess the PCNA fold, it follows that these proteins could form a complex by associating into a heterotrimeric DNA sliding clamp structure. Sequence similarity of all these three families to PCNA indicates that Rad1, Rad9 and Hus1 might associate in a head-to-tail manner, like monomers within the PCNA ring. However, even this constraint leaves two different possible combinations to form the head-to-tail heterotrimer. Which one of them represents the functional form?

In the Rad17^{Sc}/Ddc1^{Sc}/Mec3^{Sc} (Rad1/Rad9/Hus1) complex Mec3^{Sc} was determined to interact only with the N-terminal region (1–179) of Rad17^{Sc} (14). This leaves only one possible arrangement of the three proteins within the ring (Fig. 2). As a result, for each of the three protein families we could define regions that interact with proteins from the other two families within the ring structure (see Fig. 1). Additional support for this protein association model is given by a mutation in Rad17^{Sc}, E128K, that abolishes the interaction with Mec3^{Sc} (14) and confers DNA damage sensitivity similar to that caused by disruption of *RAD17* (33). The E128K mutation maps onto the β-strand forming an interface with another monomer in the ring structure (indicated in the Rad1–PCNA alignment in Fig. 1A; arrow in Fig. 2). It is unlikely that a single residue substitution at the surface of the protein would significantly affect protein conformation. The simplest explanation for such a dramatic biological consequence is that the E128K mutation disrupts the Rad17^{Sc}–Mec3^{Sc} interface, preventing the formation of a functional heterotrimeric structure. The residue in PCNA corresponding to position 128 in Rad17^{Sc}

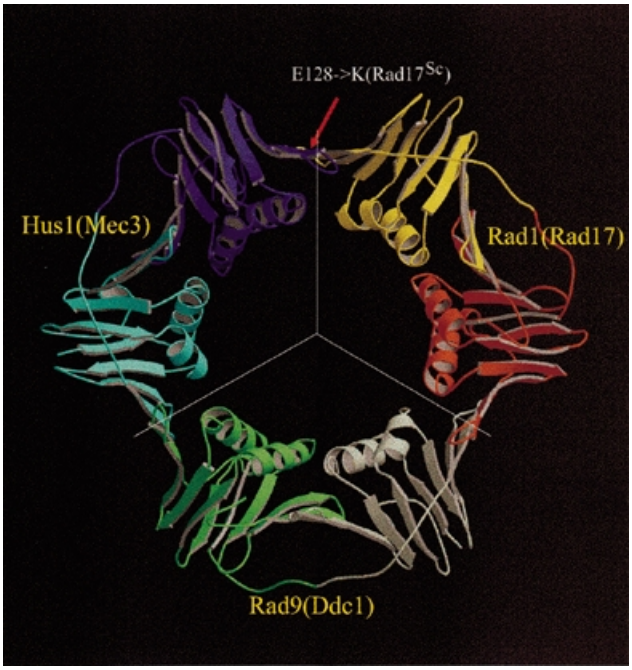

Figure 2. Model of the Rad1/Rad9/Hus1 complex based on the PCNA structure. Line segments indicate boundaries between individual monomers. Coloring corresponds to that used in sequence–structure alignments in Figure 1. The red arrow points to a residue position corresponding to a point mutation in $Rad17^{Sc}$ that prevents complex formation with $Mec3^{Sc}$. This and other structural figures were prepared with Molscript (53) and Raster3D (54).

becomes buried upon interaction with another subunit. The charge reversal at this residue position most likely prevents formation of a solvent-inaccessible salt bridge, at the same time producing very unfavorable electrostatic interaction between buried positive charges. This reasoning is also supported by the observation that single residue mutations of a corresponding β-strand in either yeast PCNA (S115P) or human PCNA (Y114A) disrupt trimer formation which eliminates PCNA activity *in vitro* and compromises yeast cell growth (36,37).

Although our modeling study combined with genetic and biochemical data indicates that the functional form of the DNA damage-responsive Rad1/Rad9/Hus1 complex is a PCNA-like heterotrimeric ring structure, a possibility exists that in addition, Rad9 and/or Hus1 may form homotrimeric clamps. However, the question of whether or not such homotrimers might be stable is beyond the sensitivity limits of our modeling analysis and cannot substitute for experimental studies.

Structure-based analysis of the Rad17 protein family nucleotide-binding function

For the checkpoint function of the Rad1, Rad9 and Hus1 proteins ($Rad17^{Sc}$, $Ddc1^{Sc}$ and $Mec3^{Sc}$), an intact Rad17 ($Rad24^{Sc}$) protein is required (14,38). The Rad17 protein family is related to subunits of clamp-loading complexes, both the eukaryotic RFC and prokaryotic γ complexes (9). Recently, an extensive sequence search and alignment study has shown that both the Rad17 family and the clamp loaders belong to a very large group of ATPases collectively designated the AAA+ class (39). Similarity between the AAA+ class proteins extends well beyond the nucleotide-binding motifs Walker A (a phosphate-binding P-loop) and Walker B (often referred to as the DEXX motif). Proteins assigned to this class feature several characteristic conserved sequence regions that distinguish them from other NTPases and fall within boxes II–VIII that were previously defined for RFC-related proteins (40).

The sequence similarity between Rad17 proteins and subunits of clamp loaders indicates structural and possible functional similarity. Of all clamp-loading proteins, an experimentally determined structure is only available for the δ′ subunit of *E.coli* polymerase III (41). The δ′ subunit is, however, unable to bind ATP and its structure does not directly elucidate the role of ATP binding and hydrolysis in the clamp-loading process. The closest structural match for the δ′ subunit is the D2 fragment of the NSF protein, another member of the AAA+ class (39), displaying similarity in topology and structure with the first two domains of δ′ (Fig. 3A). Unlike δ′, NSF D2 binds ATP with high affinity, and two independently determined high resolution structures in the ATP-bound state are available (42,43).

The close structural similarity between δ′ and NSF D2 made them both useful parent structures to derive molecular models for proteins of the Rad17 family. Although the sequence comparison suggests that Rad17 structural similarity extends throughout all three domains of δ′, the regions corresponding to the N-terminal and linker domains are more highly conserved. For these two domains, alignment of the Rad17 and RFC proteins was dubious in some of the regions; therefore, we decided to confine our modeling study to the nucleotide-binding site, where structurally equivalent motifs in both δ′ and NSF D2 also had strongly conserved sequence patterns (colored gold in Fig. 3A) that are characteristic of the entire AAA+ class (39). Those regions could be unambiguously aligned with both Rad17 and RFC protein sequences (Fig. 3B). $Rad17^{Sp}$ was chosen for modeling because some residues within its putative nucleotide-binding site have been analyzed by site-directed mutagenesis (9).

As a framework for modeling the spatial arrangement of $Rad17^{Sp}$ chain fragments, the ATP-bound form of NSF D2 was preferable over δ′. The resulting model comprises a considerable part of the $Rad17^{Sp}$ nucleotide-binding pocket (Fig. 4). From this it is apparent that $Rad17^{Sp}$ is able to preserve residue contacts with both ATP and the Mg^{2+} ion observed in the structure of NSF D2. Many of these conserved contacts involve the triphosphate moiety and come from the Walker A (P-loop), Walker B (DEXX) and Sensor-1 (41) motifs. However, the N-terminal part of the helix (Sensor-2), which comes from the second domain, also contributes several residues to the nucleotide-binding pocket. This helix, apparently conserved in both the Rad17 and RFC proteins, most likely functions to couple 'sensing' of nucleotide binding/hydrolysis with significant conformational changes.

So far, none of the members of the Rad17 family have been demonstrated to bind ATP or any other NTP. However, the reported *rad17* phenotypes arising from site-specific mutations (9) coupled with the molecular model (Fig. 4) strongly support a functional nucleotide-binding site in $Rad17^{Sp}$. The K118E mutation is responsible for loss of $Rad17^{Sp}$ function. In the

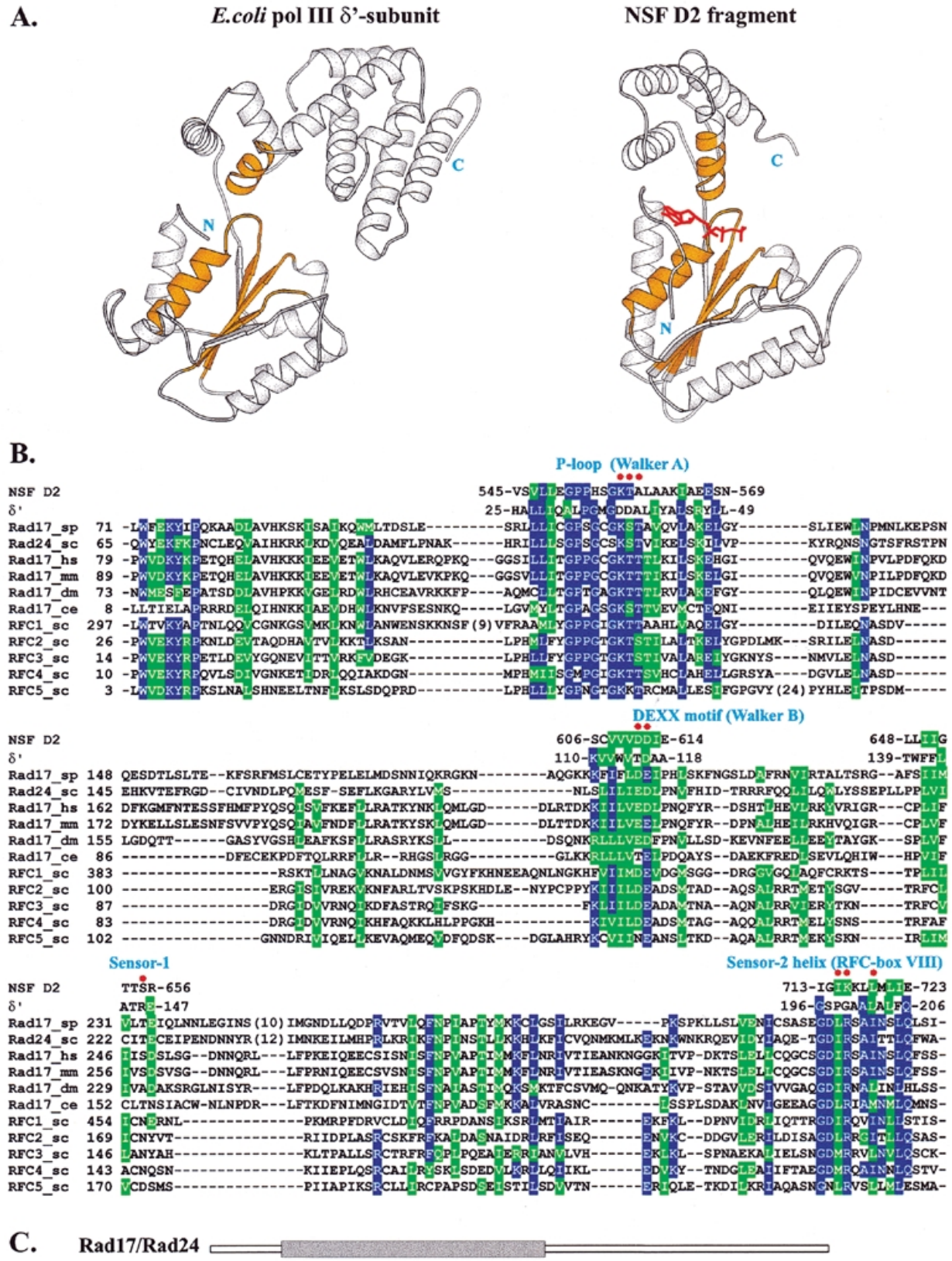
A.
E.coli pol III δ'-subunit
NSF D2 fragment
N
C
N
C
B.
P-loop (Walker A)
DEXX motif (Walker B)
Sensor-1
Sensor-2 helix (RFC-box VIII)
C.
Rad17/Rad24

model it is immediately apparent that the phosphate moiety of the nucleotide directly interacts with K118 in the P-loop and at the same time buries its side chain underneath. If Lys is substituted by Glu in this position, it would be impossible to accommodate the negatively charged Glu side chain upon nucleotide binding without creating a very unfavorable electrostatic interaction with the triphosphate. Thus, the most likely reason for abolition of function in the *rad17* K118E mutant is the inability to bind nucleotide.

In the Rad17^{Sp} model, triphosphate-binding motifs are reconstructed in full compared to NSF D2, while the nucleoside-binding pocket is modeled only partially. Although because of that we cannot be certain which NTP binds to Rad17, the relationship of the Rad17 family with RFC proteins and the AAA+ class, including NSF D2, suggests that ATP is the most likely candidate.

From this study it also appears that nucleotide binding is likely to cause significant changes in orientation between the N-terminal and linker domains. Bound ATP is sandwiched between the N-terminal domain and the Sensor-2 helix of the linker domain. In this helix two hydrophobic (L314 and I318) residues interact with the plane of the heterocyclic base and the sugar, while a positively charged residue (R315) makes contact with the phosphate moiety. In the absence of ATP these interactions are lost, and that is likely to change the orientation of the Sensor-2 helix and the whole linker domain, corresponding to that in δ′. The residues from the Sensor-2 helix interacting with ATP are part of a sequence motif highly conserved, not only in the Rad17 family, but also in RFC (referred as box VIII; 40) and other related proteins such as the prereplicative complex loader protein Cdc6 (44). RuvB helicase has also been found to share a similar motif (41). Not unexpectedly, δ′, which is defective in nucleotide binding, has different residues at the corresponding positions. A mutation in the box VIII region renders *rad17* cells more sensitive to ionizing radiation (9). Interestingly, a DNA replication defect caused by a mutation in the same region of RFC$_1$ could be suppressed by mutant PCNA proteins which contain substitutions that destabilize the homotrimeric sliding DNA clamp (45). This finding suggests that in RFC1, the region corresponding to the Sensor-2 helix in the Rad17^{Sp} model is directly involved in PCNA ring opening while it is loaded onto DNA. Although the Sensor-1 motif was also previously suggested to 'sense' ATP binding (41), its role seems to be quite different from that of the Sensor-2 helix. A comparison of δ′ and NSF D2 reveals that the Sensor-1 motif in both structures has a similar conformation, indicating that nucleotide binding has a negligible structural effect. Instead, the side chain of the Sensor-1 residue, corresponding to Rad17^{Sp} T233, appears to be important for ATPase activity, as its close position to the ATP phosphate would enable it to coordinate a water molecule for nucleophilic attack.

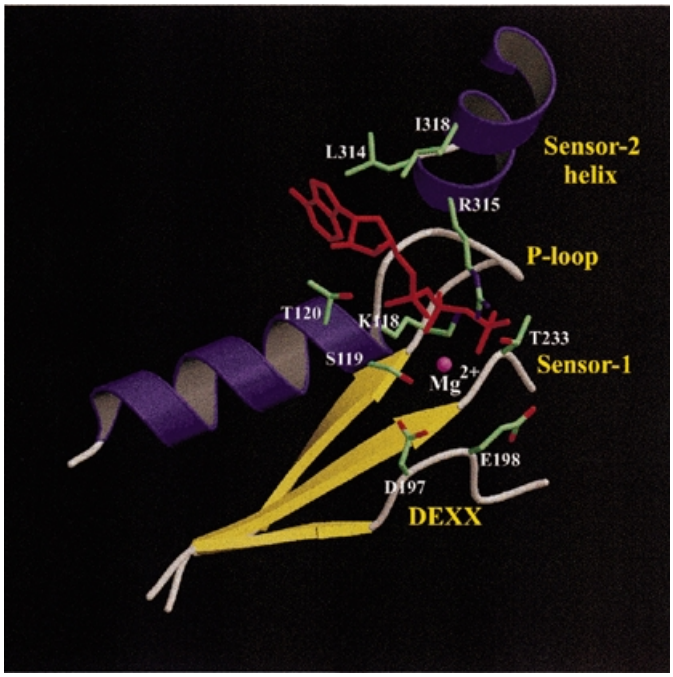

Figure 4. Model of the Rad17^{Sp} nucleotide-binding site. Side chains considered to be important for either binding ATP (red) or coordinating the magnesium ion (purple sphere) are shown for the same residues as those labeled in Figure 3B.

The model of the ATP-binding site for Rad17 from fission yeast has all the attributes of an active ATP hydrolase, including canonical P-loop and DEXX motifs. Interestingly, other members of the Rad17 protein family and RFC$_5$ all feature a modified DEXX motif. Most of them have a conservative substitution, Glu→Asp, however, in *C.elegans* Rad17 and yeast RFC$_5$ the negative charge is removed altogether by a substitution with Thr and Asn, respectively. The acidic nature of the first residue in the DEXX motif is known to be critical for catalytic activity (46), suggesting that neither *C.elegans* Rad17 nor yeast RFC$_5$ are able to hydrolyze nucleoside triphosphates.

Proposed function of the Rad1/Rad9/Hus1 and the Rad17/RFC complexes

As a result of this study, two structural models emerge to describe the Rad1, Rad9, Hus1 and Rad17 protein families. Rad1, Rad9 and Hus1 are all predicted to have the PCNA fold and furthermore to form a PCNA-like heterotrimeric DNA clamp. Rad17 family proteins are predicted to bind ATP and at

Figure 3. (Opposite) (**A**) Comparison of 3D structures of the δ′ subunit of *E.coli* polymerase III and the NSF D2 fragment. Equivalent structural motifs involved in forming the nucleotide-binding site that could also be unambiguously aligned with the Rad17 and RFC families are colored gold. The ATP analog bound to NSF D2 is shown in red. (**B**) Alignment of the Rad17 family and all five yeast RFC subunits with the structural fragments of both δ′ and NSF D2, colored gold in (A), subsequently used to construct the model for Rad17^{Sp} given in Figure 4. Residues conserved in more than half of the sequences are colored blue (identical) and green (similar). Red dots indicate Rad17^{Sp} nucleotide-binding site residues shown with their side chains in Figure 4. Numbers indicate positions of residues in sequences. (**C**) Location of the Rad17 (Rad24^{Sc}) region (gray rectangle) aligned in (B), found to be common to the AAA+ class (39).

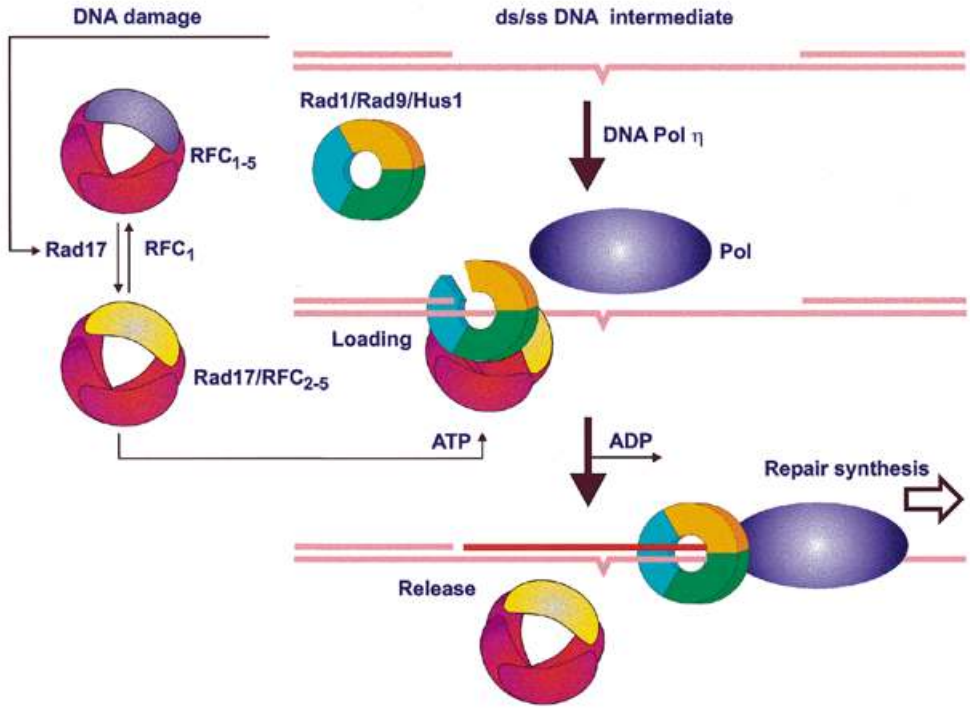

Figure 5. Proposed mechanism of Rad1, Rad9, Hus1 and Rad17 action in response to DNA damage. The DNA intermediate contains an unrepaired damaged site, such as a pyrimidine dimer (denoted by a bulge in the lower strand), that initiates translocation of Rad17 throughout the nucleus. Conversion of RFC_{1-5} to $Rad17/RFC_{2-5}$ is required for ATP-dependent loading of the Rad1/Rad9/Hus1 heterotrimeric ring onto DNA. Repair synthesis can then proceed by (for example) a lesion bypass polymerase that utilizes the heterotrimeric ring for more efficient and/or accurate synthesis. See text for a more detailed description and references.

least some of these proteins will hydrolyze it. Their close evolutionary relationship to clamp loaders, paralleled with their requirement to fulfill Rad1/Rad9/Hus1 function, strongly supports a model similar to that for function of RFC/PCNA. In such a model, the clamp-loading complex containing Rad17 ($Rad24^{Sc}$) would bind both damaged DNA and the Rad1/Rad9/Hus1 complex in an ATP-dependent fashion, and use conformational changes associated with ATP binding, hydrolysis and dissociation to break the trimer ring, load the complex onto DNA and then reseal it. Then, like PCNA, the Rad1/Rad9/Hus1 complex would provide processivity for DNA repair (or degradation) proteins, for example a lesion bypass polymerase such as Pol η (47,48; Fig. 5). In a separate, DNA damage-dependent cell cycle arrest function, the critical signal transmission role of Rad1, Rad9 and Hus1 might also be realized upon forming a clamp, topologically bound to DNA. The Rad1/Rad9/Hus1 complex might then serve as a structural mediator for initiation of a regulatory cascade of checkpoint kinases by transiently recruiting protein kinases and their phosphorylation targets such as $Rad3^{Sp}/Cds1^{Sp}$ ($Mec1^{Sc}/Rad53^{Sc}$).

Recently, some clues as to the oligomeric state of the Rad17 family members have been revealed. $Rad24^{Sc}$ has been found in a complex with all RFC subunits except for the largest subunit, RFC_1 (5), indicating that $Rad24^{Sc}$ and RFC_1 are competing for interaction with the other four RFC subunits. This idea is further supported by the fact that overexpression of $Rad24^{Sc}$ intensifies the growth defects in RFC_1 mutant cells (10), which can be interpreted as an inability of the resulting $Rad24^{Sc}/RFC_{2-5}$ complex to load PCNA. The estimated size of the RFC_{2-5} complex with $Rad24^{Sc}$ indicates that it is a pentamer, consisting of single copies of $Rad24^{Sc}$ and each of the four RFC subunits (5). $Rad17^{Sp}$ has also been found in a complex with RFC subunits (6) and the size estimated for such a complex (49) is consistent with a $Rad17^{Sp}/RFC_{2-5}$ structure. Sequence homology of Rad17 family members to RFC proteins also indicates that the quaternary structure of the Rad17/RFC complex might be very similar to that formed exclusively by RFC subunits. Conformational changes in the subunits of the Rad17/RFC complex associated with ATP binding/hydrolysis, like that predicted for $Rad17^{Sp}$, could break the Rad1/Rad9/Hus1 heterotrimer ring, allowing loading of this complex onto DNA. After ATP hydrolysis, dissociation of ADP from the Rad17/RFC complex may reseal the Rad1/Rad9/Hus1 complex.

The balance between the two types of RFC complexes might be achieved by redistribution of a Rad17 family protein within the nucleus, depending on the presence of DNA damage (8). In addition, these two RFC complexes might have different affinities for particular DNA structures. It is postulated that the 'normal' RFC complex recognizes DNA template/RNA primer junction with subsequent PCNA recruitment (50). Upon DNA damage many different DNA lesions are converted into single-stranded DNA. The RFC complex containing Rad17 might have a higher affinity for nicked or gapped DNA

as opposed to a DNA–RNA hybrid (primed DNA). The latter is expected to assume the A-form, while the DNA double helix is normally in the B-form. Such differences might determine which one of the two RFC complexes will bind to the specific structure and which DNA clamp will be loaded (either PCNA or Rad1/Rad9/Hus1).

The sliding clamp model indicates that the Rad1/Rad9/Hus1 complex could provide a platform to allow other DNA repair/synthesis/degradation enzymes to repair DNA lesions in a processive manner. Unlike PCNA, such a DNA clamp would be formed by non-identical subunits, making it more flexible in the choice of interacting partners. It is also likely that each of the Rad1, Rad9 and Hus1 proteins has an additional cellular role, extending beyond their function as components of a DNA sliding clamp. One example of this is the nuclease activity found in some Rad1 family members (35,51,52).

ACKNOWLEDGEMENTS

The authors are grateful to Drs Michael Brodsky and Gerald Rubin at the University of California Berkeley for the *Drosophila* cDNA sequences used in the alignments here, to Dr Krzysztof Fidelis for funding to C.V. and to Drs David M. Wilson, Michael Colvin and William K. Holloman for insightful comments on the manuscript. This research was additionally funded by an individual research grant from the US DOE to M.P.T. and was performed under the auspices of the US DOE by the Lawrence Livermore National Laboratory under contract no. W-7405-ENG-48.

REFERENCES

1. Longhese,M.P., Foiani,M., Muzi-Falconi,M., Lucchini,G. and Plevani,P. (1998) *EMBO J.*, **17**, 5525–5528.
2. Weinert,T. (1998) *Curr. Opin. Genet. Dev.*, **8**, 185–193.
3. Huberman,J.A. (1999) *Prog. Nucleic Acid Res. Mol. Biol.*, **62**, 369–395.
4. Caspari,T., Dahlen,M., Kanter-Smoler,G., Lindsay,H.D., Hofmann,K., Papadimitriou,K., Sunnerhagen,P. and Carr,A.M. (2000) *Mol. Cell. Biol.*, **20**, 1254–1262.
5. Green,C.M., Erdjument-Bromage,H., Tempst,P. and Lowndes,N.F. (2000) *Curr. Biol.*, **10**, 39–42.
6. Shimada,M., Okuzaki,D., Tanaka,S., Tougan,T., Tamai,K.K., Shimoda,C. and Nojima,H. (1999) *Mol. Biol. Cell*, **10**, 3991–4003.
7. Zhang,G., Gibbs,E., Kelman,Z., O'Donnell,M. and Hurwitz,J. (1999) *Proc. Natl Acad. Sci. USA*, **96**, 1869–1874.
8. Chang,M.S., Sasaki,H., Campbell,M.S., Kraeft,S.K., Sutherland,R., Yang,C.Y., Liu,Y., Auclair,D., Hao,L., Sonoda,H., Ferland,L.H. and Chen,L.B. (1999) *J. Biol. Chem.*, **274**, 36544–36549.
9. Griffiths,D.J., Barbet,N.C., McCready,S., Lehmann,A.R. and Carr,A.M. (1995) *EMBO J.*, **14**, 5812–5823.
10. Lydall,D. and Weinert,T. (1997) *Mol. Gen. Genet.*, **256**, 638–651.
11. Parker,A.E., Van de Weyer,I., Laus,M.C., Verhasselt,P. and Luyten,W.H. (1998) *J. Biol. Chem.*, **273**, 18340–18346.
12. Volkmer,E. and Karnitz,L.M. (1999) *J. Biol. Chem.*, **274**, 567–570.
13. St Onge,R.P., Udell,C.M., Casselman,R. and Davey,S. (1999) *Mol. Biol. Cell*, **10**, 1985–1995.
14. Kondo,T., Matsumoto,K. and Sugimoto,K. (1999) *Mol. Cell. Biol.*, **19**, 1136–1143.
15. Paciotti,V., Lucchini,G., Plevani,P. and Longhese,M.P. (1998) *EMBO J.*, **17**, 4199–4209.
16. Thelen,M.P., Venclovas,C. and Fidelis,K. (1999) *Cell*, **96**, 769–770.
17. Aravind,L., Walker,D.R. and Koonin,E.V. (1999) *Nucleic Acids Res.*, **27**, 1223–1242.
18. Zuccola,H.J., Filman,D.J., Coen,D.M. and Hogle,J.M. (2000) *Mol. Cell*, **5**, 267–278.
19. Altschul,S.F., Madden,T.L., Schaffer,A.A., Zhang,J., Zhang,Z., Miller,W. and Lipman,D.J. (1997) *Nucleic Acids Res.*, **25**, 3389–3402.
20. Henikoff,S. and Henikoff,J.G. (1992) *Proc. Natl Acad. Sci. USA*, **89**, 10915–10919.
21. Jones,D.T. (1999) *J. Mol. Biol.*, **292**, 195–202.
22. Fischer,D. and Eisenberg,D. (1996) *Protein Sci.*, **5**, 947–955.
23. Venclovas,C., Ginalski,K. and Fidelis,K. (1999) *Proteins*, Suppl. 3, 73–80.
24. Šali,A. and Blundell,T.L. (1993) *J. Mol. Biol.*, **234**, 779–815.
25. Bower,M.J., Cohen,F.E. and Dunbrack,R.L.,Jr (1997) *J. Mol. Biol.*, **267**, 1268–1282.
26. Sippl,M.J. (1993) *Proteins*, **17**, 355–362.
27. Bucher,P., Karplus,K., Moeri,N. and Hofmann,K. (1996) *Comput. Chem.*, **20**, 3–23.
28. Dunbrack,R.L.,Jr (1999) *Proteins*, Suppl. 3, 81–87.
29. Jones,D.T., Tress,M., Bryson,K. and Hadley,C. (1999) *Proteins*, Suppl. 3, 104–111.
30. Wood,T.C. and Pearson,W.R. (1999) *J. Mol. Biol.*, **291**, 977–995.
31. Kong,X.P., Onrust,R., O'Donnell,M. and Kuriyan,J. (1992) *Cell*, **69**, 425–437.
32. Lydall,D. and Weinert,T. (1995) *Science*, **270**, 1488–1491.
33. Siede,W., Nusspaumer,G., Portillo,V., Rodriguez,R. and Friedberg,E.C. (1996) *Nucleic Acids Res.*, **24**, 1669–1675.
34. Longhese,M.P., Paciotti,V., Fraschini,R., Zaccarini,R., Plevani,P. and Lucchini,G. (1997) *EMBO J.*, **16**, 5216–5226.
35. Naureckiene,S. and Holloman,W.K. (1999) *Biochemistry*, **38**, 14379–14386.
36. Ayyagari,R., Impellizzeri,K.J., Yoder,B.L., Gary,S.L. and Burgers,P.M. (1995) *Mol. Cell. Biol.*, **15**, 4420–4429.
37. Jonsson,Z.O., Podust,V.N., Podust,L.M. and Hubscher,U. (1995) *EMBO J.*, **14**, 5745–5751.
38. Rhind,N. and Russell,P. (1998) *Curr. Opin. Cell Biol.*, **10**, 749–758.
39. Neuwald,A.F., Aravind,L., Spouge,J.L. and Koonin,E.V. (1999) *Genome Res.*, **9**, 27–43.
40. Cullmann,G., Fien,K., Kobayashi,R. and Stillman,B. (1995) *Mol. Cell. Biol.*, **15**, 4661–4671.
41. Guenther,B., Onrust,R., Sali,A., O'Donnell,M. and Kuriyan,J. (1997) *Cell*, **91**, 335–345.
42. Lenzen,C.U., Steinmann,D., Whiteheart,S.W. and Weis,W.I. (1998) *Cell*, **94**, 525–536.
43. Yu,R.C., Hanson,P.I., Jahn,R. and Brunger,A.T. (1998) *Nature Struct. Biol.*, **5**, 803–811.
44. Perkins,G. and Diffley,J.F. (1998) *Mol. Cell*, **2**, 23–32.
45. Beckwith,W.H., Sun,Q., Bosso,R., Gerik,K.J., Burgers,P.M. and McAlear,M.A. (1998) *Biochemistry*, **37**, 3711–3722.
46. Pause,A. and Sonenberg,N. (1992) *EMBO J.*, **11**, 2643–2654.
47. Masutani,C., Kusumoto,R., Yamada,A., Dohmae,N., Yokoi,M., Yuasa,M., Araki,M., Iwai,S., Takio,K. and Hanaoka,F. (1999) *Nature*, **399**, 700–704.
48. Johnson,R.E., Prakash,S. and Prakash,L. (1999) *Science*, **283**, 1001–1004.
49. Griffiths,D., Uchiyama,M., Nurse,P. and Wang,T.S. (2000) *J. Cell Sci.*, **113**, 1075–1088.
50. Waga,S. and Stillman,B. (1998) *Annu. Rev. Biochem.*, **67**, 721–751.
51. Thelen,M.P., Onel,K. and Holloman,W.K. (1994) *J. Biol. Chem.*, **269**, 747–754.
52. Parker,A.E., Van de Weyer,I., Laus,M.C., Oostveen,I., Yon,J., Verhasselt,P. and Luyten,W.H. (1998) *J. Biol. Chem.*, **273**, 18332–18339.
53. Kraulis,P.J. (1991) *J. Appl. Crystallogr.*, **24**, 946–950.
54. Merritt,E.A. and Bacon,D.J. (1997) *Methods Enzymol.*, **277**, 505–524.